Coupling Correction in the KEK-ATF Using Orbit Response Matrix Analysis*

A. Wolski†
Lawrence Berkeley National Laboratory, Berkeley, CA 94720

J. Nelson, M.C. Ross, M.D. Woodley
SLAC, Menlo Park, CA 94025

Y. Honda
KEK, Tsukuba, Japan

(Dated: March 3, 2005)

Orbit Response Matrix (ORM) analysis is a technique used to diagnose and correct optics errors in storage rings. We report the results obtained from the use of ORM analysis at the KEK-ATF to reduce the equilibrium vertical emittance. Measurements of the vertical beam size using a laser wire indicate that the vertical emittance was successfully reduced from 12 pm to around 6 pm (at a bunch charge of 7×10^9 particles) using ORM analysis.

I. INTRODUCTION

The KEK-ATF [1] is a test facility for future linear collider damping rings. The main storage ring has a circumference of 138 m, and stores up to three trains of 20 bunches of electrons at 1.28 GeV. One of the main goals for the experimental program at the KEK-ATF is to demonstrate the vertical emittance of 2 pm specified for the International Linear Collider (ILC). This is a challenging target, and requires an improvement in coupling correction by a factor of two over the best results obtained so far [2]. Coupling correction based on Orbit Response Matrix (ORM) analysis has been applied successfully to reduce the vertical emittance in the LBNL-ALS to around 5 pm [3]. Previous attempts to apply the technique in the KEK-ATF met with mixed success [4, 5]; simulation studies suggest that the reason for this was an incorrect weighting applied to the vertical dispersion in fitting the lattice model to the measured data. In recent experimental studies, we re-applied the ORM analysis to the KEK-ATF, using a weight in fitting the vertical dispersion determined from the simulation studies. Measurements of the vertical emittance using a laser wire indicate rather better success than previous efforts.

In this note, we first describe the correction strategy (based on ORM analysis) that we applied in our recent experiments. We then discuss the results of simulation studies, and finally present the recent experimental results.

*This work was supported by the Director, Office of Science, High Energy Physics, U.S. Department of Energy under Contract Nos. DE-AC03-76SF00098 and DE-AC03-76SF00515.
†Electronic address: awolski@lbl.gov

II. ORBIT RESPONSE MATRIX ANALYSIS

The orbit response matrix (ORM) of a storage ring is constructed from the change in orbit at each beam position monitor in response to a variation in strength of each orbit correction magnet around the ring. In general, the ORM includes both in-plane elements (horizontal BPM response to horizontal correctors, and vertical BPM response to vertical correctors) and cross-plane elements (horizontal BPM response to vertical correctors, and vertical BPM response to horizontal correctors). The measured ORM contains information about the optics (for example, focusing and coupling errors) and the diagnostic system (for example BPM gain errors). ORM analysis involves taking a measured orbit response matrix, and fitting parameters in a lattice model to reproduce the measured ORM. Fitting parameters can include optics and diagnostics errors. Generally, the fit of the model to the measured data is over-constrained, which means that the technique is capable in principle of being used to determine real errors. In particular cases, however, it may be desirable to project errors from their real sources onto components available for correction. For example, coupling errors may arise from vertical sextupole misalignments, and quadrupole rotations about the beam axis. Such errors may be determined from the ORM analysis, but if the aim is to correct the errors using a given set of skew quadrupoles, the lattice model may be fitted to the ORM data by localizing all the coupling errors at the skew quadrupoles, and treating the sextupoles and quadrupoles as if they were correctly aligned. If a good fit is still obtained to the measured ORM, then the skew quadrupole strengths obtained in the fit may be used to determine a coupling correction. This is the strategy that we applied in the KEK-ATF to reduce the vertical emittance.

One potential problem with an analysis based purely on the orbit response matrix is the degeneracy between the BPM gains and corrector strengths. This degeneracy may be resolved by including the measured dispersion in

the fit, which provides information on the BPMs independent of the orbit correction magnets. In a machine such as the KEK-ATF, where the nominal vertical dispersion is zero, the question then arises as to how to treat the measured vertical dispersion. This is particularly important where the aim is to reduce the vertical emittance, as in the present case. Vertical dispersion can arise from vertical steering errors as well as from coupling, but the ORM analysis does not model the orbit distortion directly. Accurate results for the coupling will only be obtained if the weight applied to the vertical dispersion in the fit reflects the contribution of the coupling (as opposed to the vertical steering) to the measured vertical dispersion. The appropriate weight may be determined by simulations of the ORM analysis, using errors representative of those expected in the real machine. Detailed simulations performed in advance of recent experimental work at the KEK-ATF indicated that previous attempts to correct the coupling using ORM analysis may not have been fully successful because the weight applied to the vertical dispersion in fitting the coupling errors was likely too small. Results from the more recent work, using a significantly larger weight for the vertical dispersion, indicate rather better success in reducing the vertical emittance. The results of the simulations and the experiments are reported below.

For ORM analysis at the KEK-ATF, we used the MATLAB version of the code LOCO developed by Safranek *et al* [6].

III. SIMULATIONS

To determine the optimum values of various parameters for the analysis of the measured KEK-ATF orbit response matrix, we performed simulations of the analysis using known optics and diagnostics errors. The errors were chosen to represent the state of the machine after initial tuning for orbit, dispersion and coupling correction, and included: quadrupole focusing errors; quadrupole vertical misalignments; quadrupole roll errors; skew quadrupole errors superposed on the sextupoles (representing vertical sextupole misalignments); BPM gain and coupling errors; corrector magnet strength and roll errors. After applying a given set of errors to the machine model, an orbit response matrix was calculated, and fitted using LOCO. In the fit, all coupling errors (primarily quadrupole rolls and sextupole misalignments) were projected onto a set of skew quadrupoles used in the real machine for coupling correction. The fitted strengths of the skew quadrupoles were used to determine a coupling correction. The errors found from the ORM analysis were compared to the applied errors, and the effect of the coupling correction was estimated from the beam tilt and vertical beam size in the model before and after correction. The procedure was repeated for a given set of errors, using a range of weights on the vertical dispersion, and the entire process was repeated for a number of seeds of errors.

In the KEK-ATF, coupling correction is achieved using skew quadrupole trim windings on the sextupoles. The sextupoles are arranged in two families (SF and SD) of 34 magnets each, and are needed for chromaticity correction. Each skew quadrupole is individually powered. Each arc cell has one SF sextupole and one SD sextupole; within each cell, the sextupoles are in close proximity and the horizontal and vertical phase advances between them are similar. In consequence, the skew quadrupoles are approximately degenerate in terms of their effect on the coupling. If the strengths of all skew quadrupoles are used as parameters in the ORM analysis, the result is generally that the fitted skew strengths are extremely large, but with the skew quadrupoles on the SD sextupoles approximately cancelling those on the SF sextupoles. Using only the skew quadrupoles on either the SF or SD sextupoles still results in a good fit of the model to the simulated (or measured) ORM, but with realistic strengths for the skew quadrupoles. The choice of whether to use the skew quadrupoles on the SF or SD sextupoles is arbitrary; we generally use the skew correctors on the SF sextupoles.

Typical results from a simulation of the ORM analysis are shown in Figs. 1 - 7. Fig. 1 shows the orbit response matrix in the model with one seed of machine errors, and the difference between the calculated ORM and the ORM in the model fitted using ORM analysis. Note that the cross-plane terms in the response matrix are small compared to the in-plane terms. The quality of the fit can be seen from the difference in vertical scale between the two plots. The quality of the fit is not sensitive to the weight applied to the vertical dispersion in the ORM analysis; in this case, a weight of 20 was applied.

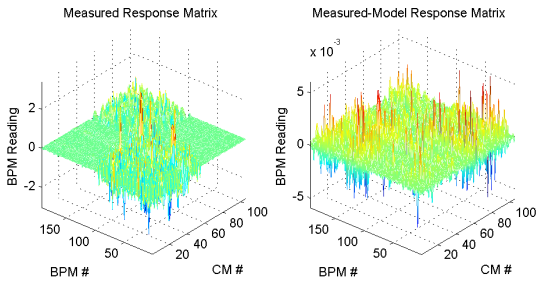

FIG. 1: Simulated ORM (left) and difference between the calculated ORM and that of the model fitted by the ORM analysis (right).

Fig. 2 shows the applied and fitted focusing errors on the quadrupoles, and the applied and fitted skew errors on the SF sextupoles. The focusing errors are fitted very well, but there appears to be a poor fit to the skew errors.

The reason for this is that the coupling errors come from several sources, including orbit offset in the sextupoles, skew errors on both SF and SD sexupole families, and quadrupole rolls. The fit projects all these errors onto the skew quadrupoles on the SF magnets, for purposes of determining the appropriate coupling correction.

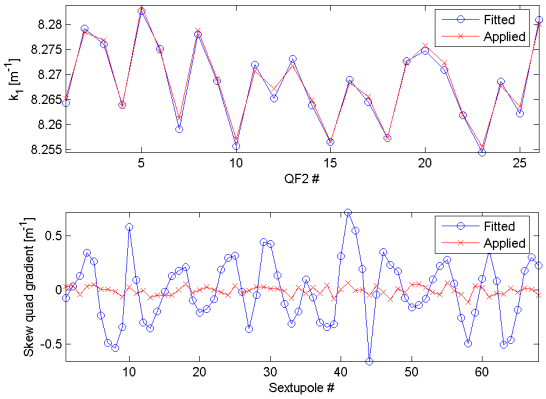

FIG. 2: Comparison between focusing errors (top) and skew quadrupole errors (bottom) applied in simulation, and errors determined from ORM analysis.

Fig. 3 shows a comparison between the applied and fitted BPM gain errors in the simulation, and Fig. 4 shows a comparison between the applied and fitted BPM coupling errors. Note that the BPM gain and coupling errors are defined as components of a matrix g that relates the actual beam position to the beam position measured by the BPM:

$$\begin{pmatrix} x \\ y \end{pmatrix}_{\mathrm{BPM}} = \begin{pmatrix} g_{xx} & g_{xy} \\ g_{yx} & g_{yy} \end{pmatrix} \cdot \begin{pmatrix} x \\ y \end{pmatrix}_{\mathrm{beam}} \qquad (1)$$

g_{xx} and g_{yy} are the horizontal and vertical gains respectively; g_{xy} and g_{yx} are the couplings. If the couplings arise from a mechanical rotation of the BPM, then the coupling components are related. In general, we make no assumptions about the origin of the coupling, and allow the components g_{xy} and g_{yx} to be independent. We see from Figs. 3 and 4 that the BPM gains and couplings are fitted with very good accuracy, as was typical in all the simulation cases we looked at.

Fig. 5 shows the corrector kicks applied in simulation when calculating the orbit response matrix, and the corrector kicks determined from the ORM analysis. As with the BPM gains and couplings, the corrector kicks are fitted with very good accuracy.

Fig. 6 shows the vertical dispersion in the lattice model with applied steering and coupling errors compared with the vertical dispersion in the model fitted using ORM. The fitted model includes only coupling errors, and no steering errors. The steering errors applied were sufficient to generate a closed orbit distortion with an rms of several hundred microns; this is believed to be representative of the real machine. With the applied coupling

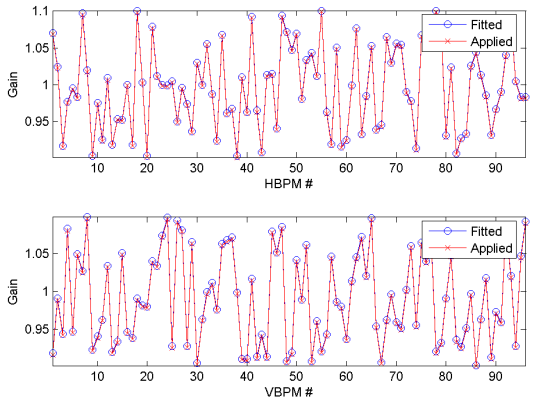

FIG. 3: Comparison between BPM gain errors applied in simulation, and errors determined from ORM analysis.

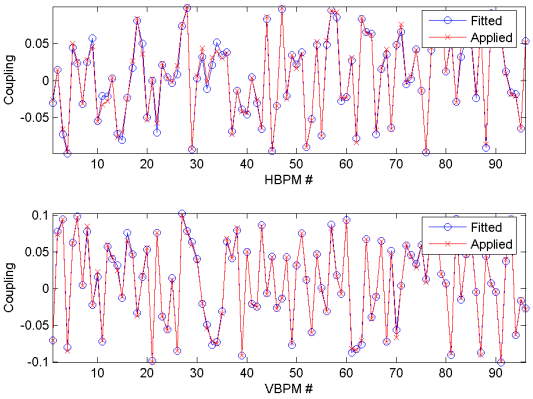

FIG. 4: Comparison between BPM coupling errors applied in simulation, and errors determined from ORM analysis.

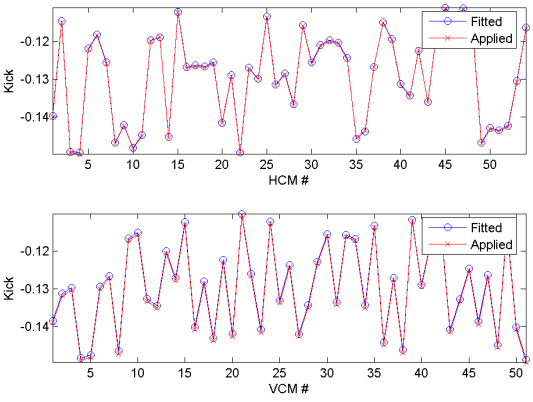

FIG. 5: Comparison between corrector kick errors applied in simulation, and errors determined from ORM analysis.

errors, which together with the steering errors generate a vertical emittance of between 10 pm and 20 pm, the vertical dispersion appears to be dominated by the coupling, and in this case is reproduced accurately by the model fitted using ORM analysis. The accuracy of the fit to the vertical dispersion depends strongly on the weight applied to the vertical dispersion in the ORM analysis. With a weight of 10 or less, the fit is generally poor. In the present case, we show the results of a fit with a weight of 20 on the vertical dispersion.

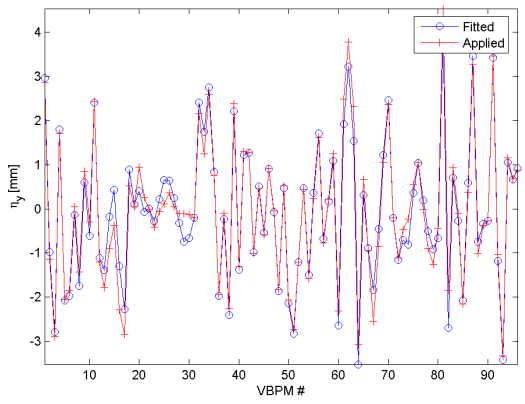

FIG. 6: Comparison between vertical dispersion in the lattice model with the applied errors, and the vertical dispersion in the lattice model fitted using ORM analysis.

Finally, Fig. 7 shows the beam tilt and equilibrium beam sizes in the model with the applied errors, before and after coupling correction. The coupling correction was determined directly from the fitted skew quadrupole strengths, shown in Fig. 2: we simply applied the reverse strengths of the fitted skew quadrupoles to the corresponding magnets in the original model. In this case, there is a signficant reduction in the coupling, with the vertical emittance reduced from more than 10 pm to less than 2 pm.

Fig. 8 summarizes the results of the ORM analysis simulation. For a given seed of machine errors, increasing the weight on the vertical dispersion in the ORM analysis leads to a more effective correction of the coupling. In the regime we consider, the vertical dispersion is dominated by the coupling, so the final vertical emittance as a function of the weight on the dispersion does not go through a minimum, but reaches a limit as a very close fit to the vertical dispersion is achieved. In the case that the vertical dispersion has a significant contribution from vertical steering, the vertical emittance is expected to increase as a result of the coupling correcion if too large a weight is placed on the vertical dispersion in the ORM analysis.

From Fig. 8, we chose a weight of 20 to apply to the vertical dispersion in the ORM analysis of the measured machine orbit response matrix. Values larger than 20 appear to give little benefit to the coupling correction, and

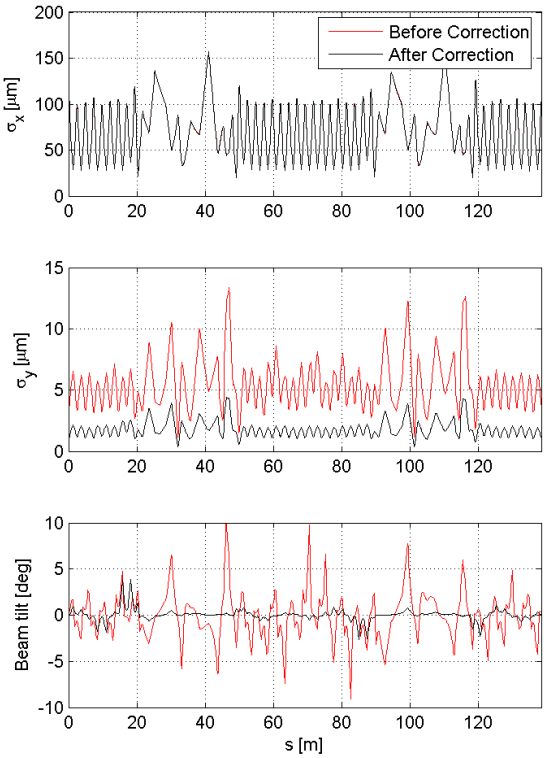

FIG. 7: Effect of coupling correction in simulation using ORM analysis. The red line shows the beam sizes and beam tilt in the lattice model with applied errors; the black line shows the beam sizes and beam tilt in the same model, but with coupling correction determined using ORM analysis.

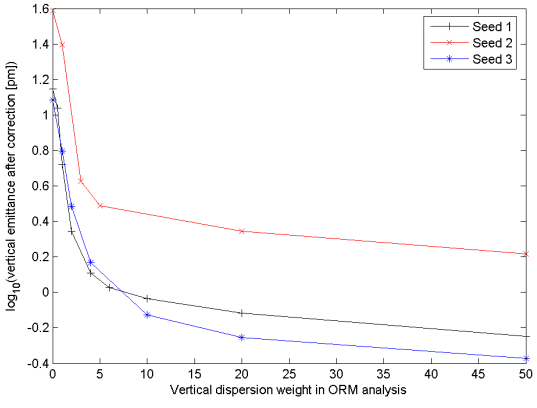

FIG. 8: Vertical emittance of lattice model with applied errors after coupling correction determined from ORM analysis. Each line corresponds to a single seed of machine errors, with different weights on the vertical dispersion in the ORM fit.

risk increasing the vertical emittance in the case that vertical steering makes a significant contribution to the vertical dispersion. In practice, we found that with a weight of 20, an accurate fit to the measured vertical dispersion could be achieved without noticeable degradation of the fit to the measured ORM. In our previous studies [4, 5], we used a weight of 1, which resulted in a poor fit to the vertical dispersion, and a coupling correction that was not very effective.

IV. EXPERIMENTAL RESULTS

Experimental data for the ORM measurement were collected using a control-system application written by K. Kubo (KEK). This application automates the variation of each of the corrector magnets over a specified range in a number of steps, and reads 10 orbits from the BPMs at each corrector step. A beam current of more than 3 mA (corresponding to a bunch charge of 8.6×10^9 particles) is generally needed for the BPMs to achieve a good resolution of less than 5 μm. The BPMs have some systematic dependence on beam current, which can affect the ORM data. The beam lifetime in the KEK-ATF is typically just three or four minutes, which means that in stored beam mode, the beam current will vary over a significant range during measurements of the orbit response for even a single corrector. For this reason, data are collected with the machine in normal operating mode, in which a single bunch is injected into the storage ring at a rate of 1.5 Hz, and the BPMs read an orbit for a single specified turn after injection. This provides a relatively constant current during the ORM measurement, although in practice, the current can vary because of shot-to-shot variations in injection performance. Orbit variations arising from the changes in corrector strength can also adversely affect injection efficiency, and typically a small number of correctors (maybe 6 out of the total of 97) must be excluded from the data set. An additional problem comes from phase noise on the RF system, which drives synchrotron oscillations and contaminates the orbit measurements with some dispersion signal. At the time we performed the studies reported here, a small number of BPMs (2 or 3 out of a total of 96 in each plane) were not functioning.

The rate of data collection for the ORM analysis is limited by the repetition rate because the BPMs can read only one orbit on each machine pulse. Because of the dependence of the BPM readings on the beam current, and the energy jitter in the stored beam, a number of orbits need to be collected and averaged for each setting of each corrector magnet. We found that 10 orbit averages produced good results. With relatively stable machine operation, a full set of ORM data may be collected in around 2 hours. If the injection is poor, or fluctuating significantly from pulse to pulse, data collection may take much longer. Fitting a machine model to the measured data using LOCO takes about 20 minutes.

During our recent studies, we collected a total of 5 sets of ORM data: two sets were taken during a single shift on January 20; one set was taken over two shifts on January 21; and a further two sets were taken on a single shift on January 25. During the shifts on January 21, injection was not stable, and the ORM data are not considered very reliable. Analysis of the second data set taken on January 25 showed a number of anomalies suggesting either a significant change in machine conditions or (more likely) a temporary failure of some of the diagnostics during data collection; this set of data was therefore discarded. After collecting each set of data, we performed the ORM analysis using LOCO and determined a coupling correction, as described in Section III, by fitting skew quadrupole components on the SF sextupoles. The coupling correction was applied, and the effectiveness estimated qualitatively by measuring the beam lifetime before and after the correction. Since the beam lifetime in the ATF is dominated by Touschek scattering, a reduction in beam lifetime indicates a reduction in vertical emittance (assuming changes to the skew quadrupoles affect only the coupling, and have no effect on the energy acceptance).

A. Skew Quadrupole Calibration

In the cases where a second set of ORM data were collected immediately after applying a coupling correction, it is possible to validate the ORM fit by comparing the known changes in skew quadrupole currents with the changes in fitted skew quadrupole gradients. The results of such a comparison for the ORM data collected on January 20 are shown in Fig. 9. There is a good correlation between the known current changes and the changes in skew quadrupole strength determined from the successive ORM fits. The gradient of a linear fit to the data points is in very good agreement with the nominal calibration of the skew quadrupoles, -0.001 m^{-1}/A.

Our attempts to apply the correction determined by the ORM analysis were constrained by the limited range available on the skew quadrupole power supplies. The nominal range on these supplies is between ±10 A, although some particular supplies were unable to go beyond ±9 A. In a small number of cases (generally 3 or 4 skew quadrupoles out of 34) the correction indicated by the ORM analysis required a skew quadrupole strength outside the available range. This was the case for corrections using both the SF and SD skew quadrupoles. Since the ORM analysis fitted the skew quadrupole strengths on either the SF magnets or the SD magnets separately and these magnets are nearly degenerate from the point of view of the coupling, it would be interesting in future studies to see whether the overall strengths could be reduced by starting from a lattice with all skew quadrupoles turned off. If it is decided that further coupling correction requires skew quadrupole strengths outside the available range, it may be pos-

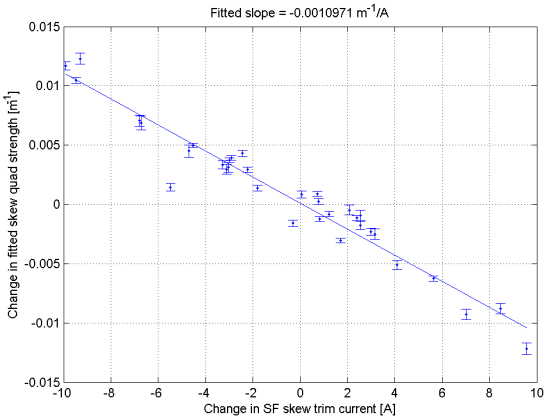

FIG. 9: Change in fitted skew quadrupole gradient between two successive ORM measurements on January 20, as a function of the known change in skew quadrupole current applied between the measurements.

sible to steer the beam to change the vertical offset in the sextupoles, or some vertical re-alignment of the sextupoles may be attempted. With the nominal sextupole strengths, a change in skew quadrupole current of 1 A corresponds to a vertical displacement of a sextupole by roughly 25 μm.

B. ORM Fits

Figs. 10 - 12 show the fit to the orbit response matrix for the first data set taken on January 25. The cross-plane terms in the ORM (shown in detail in Figs. 11 and 12) are small, and the residuals are dominated by a few "noisy" BPMs. The fit to the measured dispersion (actually, the change in measured orbit with respect to a given change in RF frequency) is shown in Fig. 13. The overall quality of the fit can be estimated from the distribution of residual differences between the measured and fitted orbit response matrices, normalized to the resolution of the respective BPMs. An "ideal" fit, in which the real machine errors are reproduced accurately in the fitted model, is expected to have a normal distribution with unit width.

The distribution of residuals for the ORM analysis for the first set of data taken on January 25 is shown in Fig. 14. The distribution has a width roughly equal to 2, which is typical of the data sets analyzed. Although this is a reasonable fit, it does indicate that there are some machine errors that are not being accurately modeled.

C. Errors in BPMs, Correctors and Quadrupoles

The fitted BPM gain and coupling errors are shown in Figs. 15 and 16 respectively. Although there is some variability in the fits to the ORM data taken at different

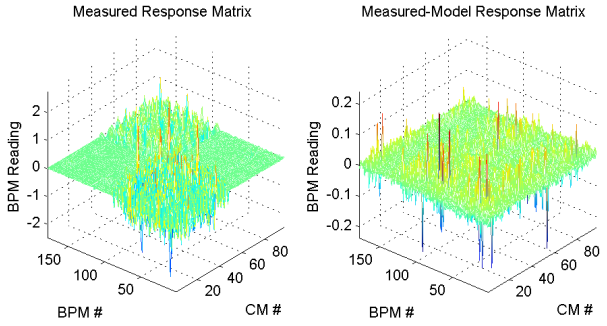

FIG. 10: Orbit response matrix measured on January 25 (left) and residuals to fitted model (right).

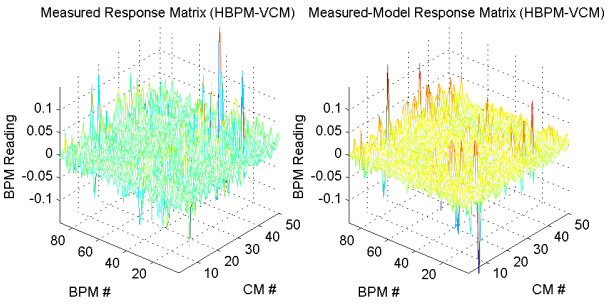

FIG. 11: Sector of the orbit response matrix measured on January 25 corresponding to horizontal BPM response to changes in vertical corrector magnet strength (left) and residuals to fitted model (right).

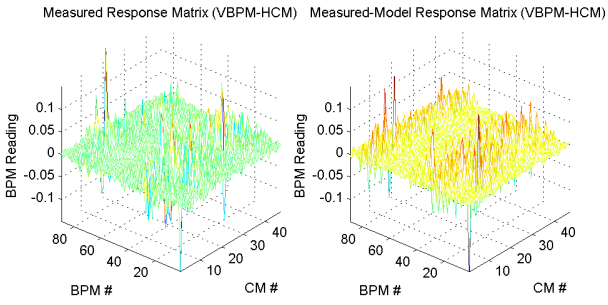

FIG. 12: Sector of the orbit response matrix measured on January 25 corresponding to vertical BPM response to changes in horizontal corrector magnet strength (left) and residuals to fitted model (right).

times, for most BPMs the values for the gains and couplings determined by the ORM analysis are reproducible with good accuracy.

The fitted corrector kicks are compared with the nominal applied kicks in Fig. 17. As with the BPMs, there is some variability in the results from different sets of ORM data, but for most correctors the kick strengths are reproducible with good accuracy.

Fig. 18 shows the quadrupole gradients determined

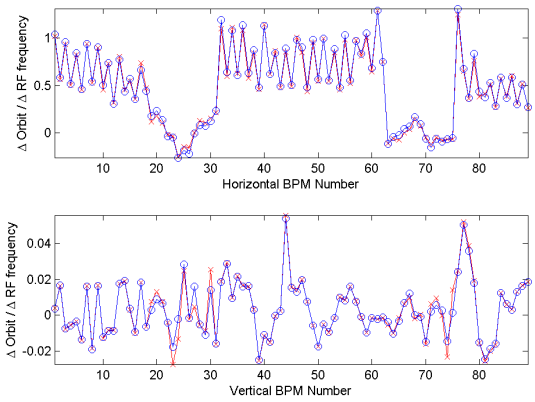

FIG. 13: Change in measured horizontal orbit (top) and vertical orbit (bottom) with respect to change in RF frequency. The red line marked with crosses shows the measured data, the blue line marked with circles shows the corresponding orbit change in the fitted model.

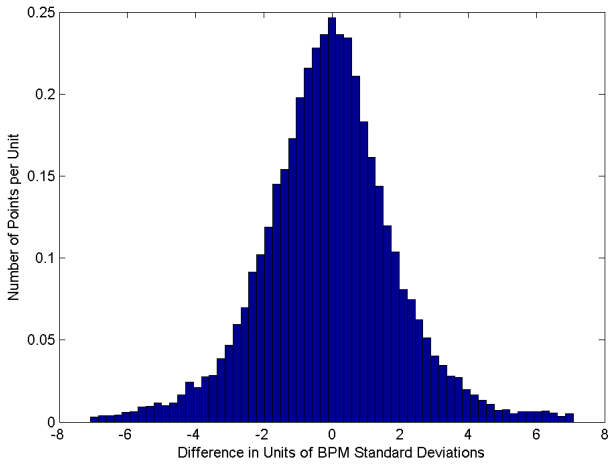

FIG. 14: Distribution of residual differences between measured and fitted orbit response matrix, normalized to the resolution of the respective BPMs.

from the ORM analysis compared to the nominal values in the original lattice model.

D. Effect of Coupling Correction on Dispersion and Beam Lifetime

The effect of the coupling correction was estimated from the change in vertical dispersion and the change in beam lifetime. The vertical dispersion was measured by varying the RF frequency and recording the change in orbit. It is important to note that the measured vertical orbit change can result from BPM coupling, as well as from real vertical dispersion. If we assume that the BPM gains and couplings determined from the ORM analysis

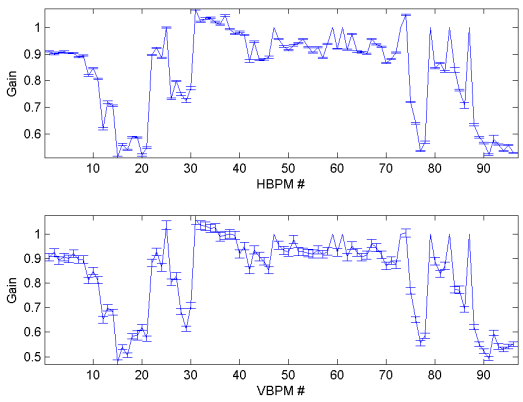

FIG. 15: Fitted BPM gains, g_{xx} (top) and g_{yy} (bottom).

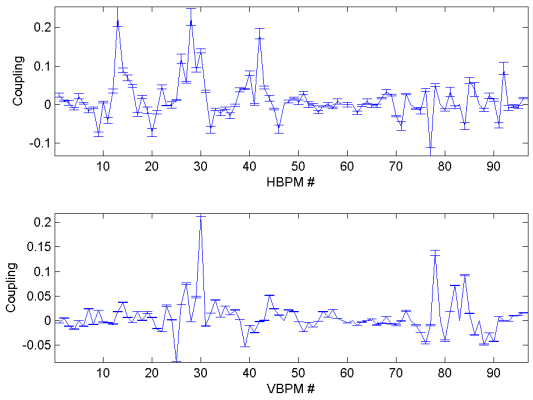

FIG. 16: Fitted BPM couplings, g_{xy} (top) and g_{yx} (bottom).

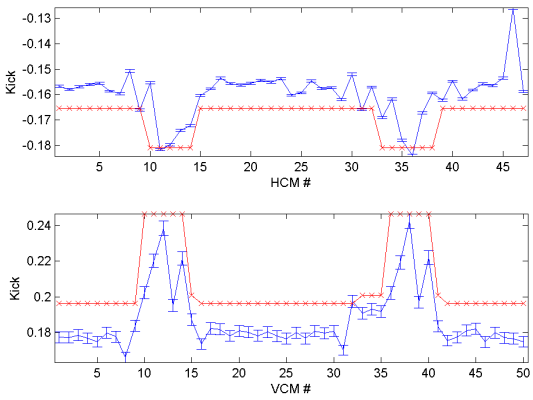

FIG. 17: Corrector horizontal kicks (top) and vertical kicks (bottom). The red line marked with crosses shows the nominal applied values; the blue line marked with circles shows the fitted values from the ORM analysis.

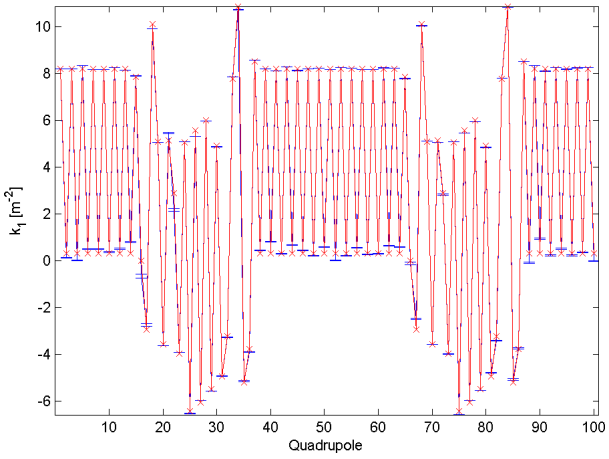

FIG. 18: Quadrupole strengths determined from ORM analysis. The red line marked with crosses shows the nominal strengths; the blue line with error bars shows the strengths in a model fitted to the orbit response matrix.

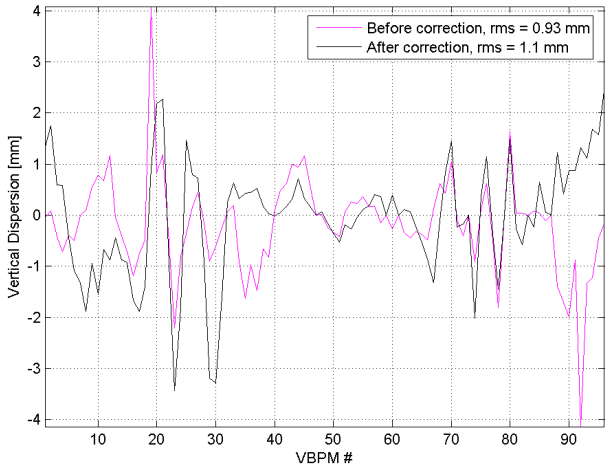

FIG. 20: Change in vertical dispersion (calculated with BPM gains and couplings determined from ORM analysis) with successive coupling corrections on January 25.

are accurate, then we can determine the real orbit motion corresponding to given changes in BPM readings by inverting Eqn. (1). Applying this correction to the data recorded on January 20, we obtain the results shown in Fig. 19. The two iterations on the coupling correction reduced the rms vertical dispersion from a little over 3 mm, to just under 1 mm. Further correction, using the ORM analysis from January 25, led to a small increase in the vertical dispersion, to a little over 1 mm, shown in Fig. 20. However, with the change in RF frequency of ± 6 kHz used in the dispersion measurement (on a nominal RF frequency of 714 MHz) and a momentum compaction of 2.1×10^{-3}, the change in vertical orbit with a dispersion of 1 mm is less than 10 μm, which is approaching the resolution of the BPMs.

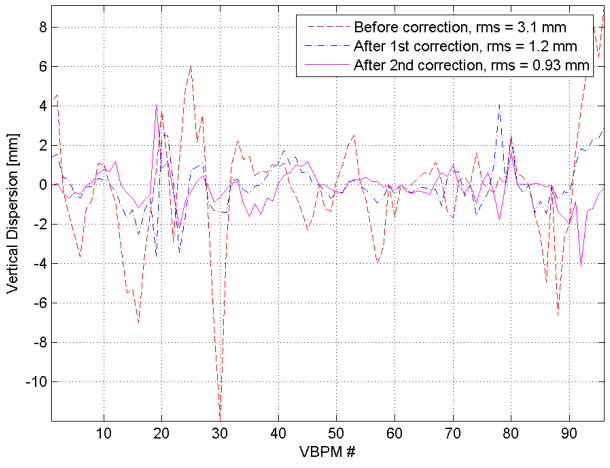

FIG. 19: Change in vertical dispersion (calculated with BPM gains and couplings determined from ORM analysis) with successive coupling corrections on January 20.

The dispersion results suggest a reduction in coupling after each correction on January 20, with little reduction in coupling thereafter. The beam lifetime measurements are consistent with this interpretation. Fig. 21 shows the beam lifetime as a function of beam current before the coupling correction, and after the two applied coupling corrections on January 20. Fig. 22 shows the beam lifetime as a function of current before and after coupling correction on January 25. With the assumption that the beam lifetime is dominated by Touschek scattering, and that adjusting the skew quadrupoles does not affect other critical parameters (such as the energy acceptance) a reduction in beam lifetime indicates a reduction in vertical emittance.

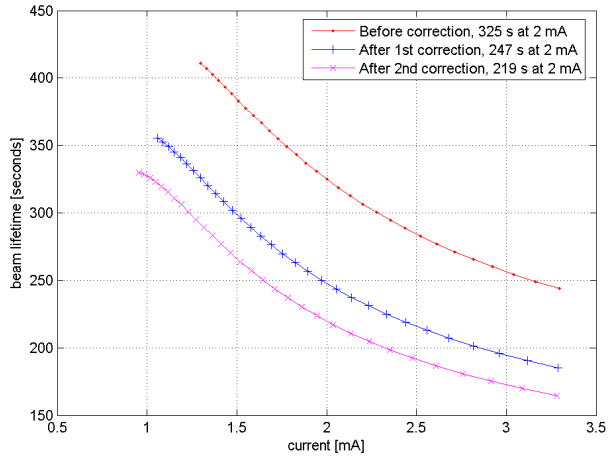

FIG. 21: Change in beam lifetime with successive coupling corrections on January 20.

We can make a rough estimate of the expected beam lifetime by assuming a constant energy acceptance

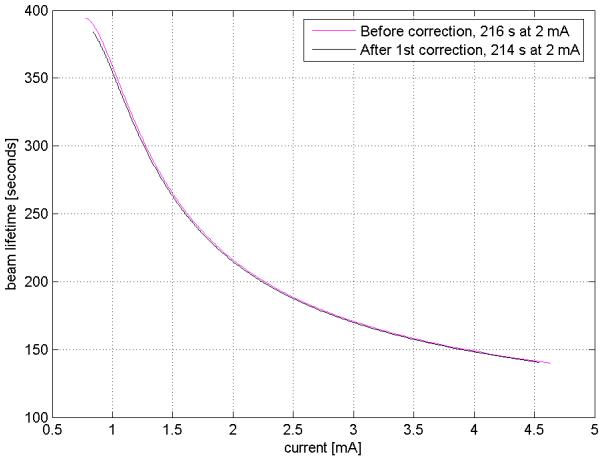

FIG. 22: Change in beam lifetime with successive coupling corrections on January 25.

around the ring. With an energy acceptance of 2%, a bunch length of 3 mm, a vertical emittance of 5 pm, and a bunch charge of 5×10^9 particles (1.74 mA), the Touschek lifetime [7] is 330 seconds. This is a little longer than the measured lifetime after coupling correction on January 20, which suggests that the real energy acceptance may be somewhat less than 2%. Assuming a vacuum pressure of 1 ntorr, with the dominant residual gas species CO, the gas scattering lifetime [8] is of the order 15 hours: the beam lifetime is clearly dominated by Touschek scattering.

E. Beam Size Measurements

The laser wire in the KEK-ATF storage ring was used to check the vertical emittance reduction with a direct beam size measurement. The beam size was measured immediately following the ORM tuning on January 25, and repeated after re-loading the lattice settings from before the ORM tuning on January 20. Set-up for laser wire measurements, including checking the laser wire condition, finding the beam signal, and checking the collimator alignment, took around 30 minutes. An initial measurement was made with the laser wire in the normal mode (TEM_{00} gaussian). The measured size was 10.96 μm, including the laser wire size of 10 μm. This result indicated that the vertical beam size was too small to measure in the normal mode, and the laser was therefore switched to the higher-order mode (TEM_{01} hermite-gaussian) which can provide a factor of 2 better resolution.

The measurement was made with the ring in storage mode, starting with a current of around 3 mA in a single bunch. When the current decreased to 2 mA, the data-taking was paused and a new bunch injected and stored. This procedure was repeated seven times, while the laser wire was scanned back-and-forth across the beam. The average beam current during the measurement was 2.49 mA; the rms of the current variation was 0.31 mA. The result is shown in the left of Fig. 23. From the fit, the beam size was found to be 4.56±0.39 μm. The error includes only statistical errors, which are expected to be dominant.

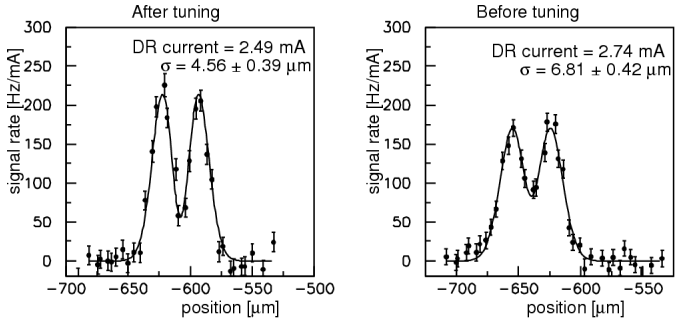

FIG. 23: Beam size measurement profile with the laser wire in TEM_01 mode. Left: after ORM coupling correction. Right: before ORM coupling correction.

The beam size measurement was repeated using the skew quadrupole settings saved prior to the ORM tuning. For these measurements, the average beam current was 2.71 mA, with an rms variation of 0.60 mA. The beam size was 6.81±0.42 μm. The results are shown in the right of Fig. 23. Note that the shallower depth of the valley between the two peaks indicates the larger size of the beam.

F. Beta Function Measurements and Emittance Estimates

After the beam size measurements, the beta functions at the laser wire position were found from the response of the betatron tunes to the variations in strength of three quadrupoles in the vicinity of the laser wire. The three quadrupoles used were QM13R.1, QM14R.1 and QM15R.1: the laser wire collision point is located 1.352 m downstream of the center of QM14R.1. The beta functions at the quadrupoles were calculated, and then the beta functions at the laser wire were found by interpolation, using a linear model in SAD. Fig. 24 shows the measured beta functions at the quadrupoles and the fitted functions used to interpolate the values at the laser wire. The vertical beta function at the laser wire was 3.23±0.1 m.

Using a value of 3.2 m for the vertical beta function at the laser wire, the beam size measurements indicate a reduction in the vertical emittance from 14.5 pm to 6.5 pm, as a result of the ORM tuning.

The beta functions at the laser wire may also be estimated from the fitted ORM models. In general, the vertical beam size has a dependence on the horizontal, vertical and longitudinal beam emittances, which may

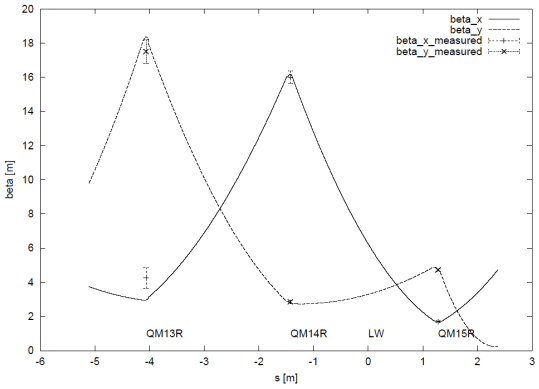

FIG. 24: Beta functions in the vicinity of the laser wire, fitted to measurements made by varying quarupole strengths.

be expressed as:

$$\sigma_y^2 = \beta_{33}^{\mathrm{I}}\epsilon_{\mathrm{I}} + \beta_{33}^{\mathrm{II}}\epsilon_{\mathrm{II}} + \beta_{33}^{\mathrm{III}}\epsilon_{\mathrm{III}} \qquad (2)$$

where ϵ_{I}, ϵ_{II} and ϵ_{III} are the invariant beam emittances and the lattice functions β_{33}^{I}, β_{33}^{II} and $\beta_{33}^{\mathrm{III}}$ may be determined from the 6×6 single-turn matrix at the chosen point in the lattice. In an uncoupled lattice the emittances may be identified with the horizontal, vertical and longitudinal degrees of freedom, and the lattice function β_{33}^{II} may be identified with the vertical beta function β_y. Since the linear optics are characterized by the orbit response matrix, we may use a model of the lattice fitted to the ORM to determine the lattice functions. This process is further justified by the close correspondence between the tunes in the fitted model and the measured tunes in the machine. As the fitting process does not make use of the tunes, good agreement between the tunes of the model and the real machine may be used to validate the fit. The tunes of the models fitted to different sets of ORM data are typically within 0.005 of the measured tune values, which are generally close to 0.192 horizontally, and 0.563 vertically.

Fig. 25 shows the lattice functions in the region of the laser wire determined from lattice models fitted to different sets of ORM data. We note that β_{33}^{I} (the vertical beam size dependence on the horizontal emittance) decreases steadily after each coupling correction. $\beta_{33}^{\mathrm{III}}$, which gives the vertical beam size dependence on the longitudinal emittance (closely related to the vertical dispersion) is reduced after each of the first three coupling corrections, but appears to increase after the third correction. This is consistent with the observed changes in vertical dispersion. With a horizontal emittance of roughly 1.1 nm, and a longitudinal emittance of roughly 1.8 μm, the horizontal and longitudinal emittances contribute approximately 10^{-12} m^2 each to σ_y^2 at the laser wire. The measured vertical beam size at the laser wire after the final coupling correction on January 25 was $\sigma_y = 4.56$ μm; so the horizontal and longitudinal emittances make negligible contribution to the vertical beam size. The lattice function β_{33}^{II} varies between 3.6 m and 3.8 m for the fits to the different sets of ORM data; the value for the fit to the final data set on January 25 was 3.6 m, which gives a vertical emittance of 5.8 pm. For the lattice before any coupling correction, the measured vertical beam size was 6.81 μm, and the lattice function β_{33}^{II} was again 3.6 m, which gives a vertical emittance of 12.9 pm. Note that the laser wire measurements were made with a bunch charge of 7×10^9 particles, at which charge a significant emittance growth from intra-beam scattering is expected [2].

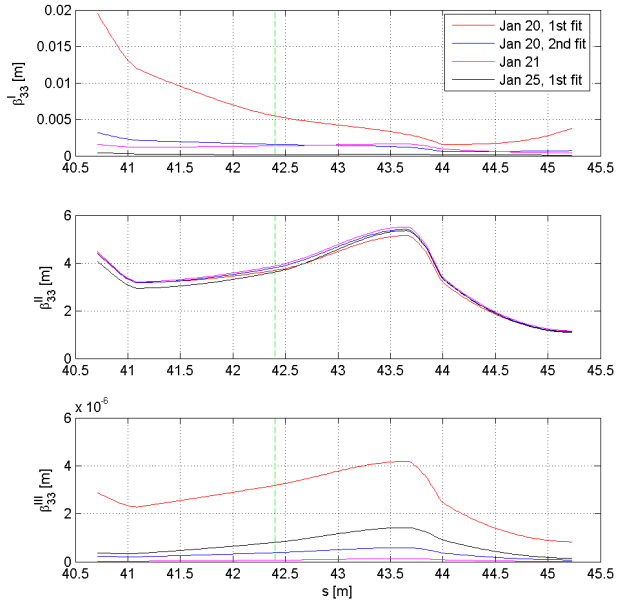

FIG. 25: Lattice functions in the vicinity of the laser wire, determined from lattice models fitted to different sets of ORM data. The position of the laser wire is indicated by the vertical broken green line.

The fitted lattice models can also be used directly to estimate the reduction in vertical emittance resulting from the coupling correction. Fig. 26 shows the equilibrium horizontal and vertical beam sizes and beam tilt calculated using the modeling code AT [9], for each of the lattice models fitted to the different sets of ORM data. The reduction in coupling from successive corrections is clearly visible. The model fitted to the data on January 25 has a vertical emittance below 2 pm: this is optimistic, even at low current.

Fig. 27 shows the growth in horizontal emittance, vertical emittance and bunch length with increasing bunch charge, resulting from intrabeam scattering (IBS). Growths starting from zero-current vertical emittances of 5.7 pm and 3.6 pm are shown (0.5% and 0.3% coupling respectively). With a bunch charge of 7×10^9, the vertical emittance with 0.3% coupling is 5.6 pm. The beam-size measurements are consistent

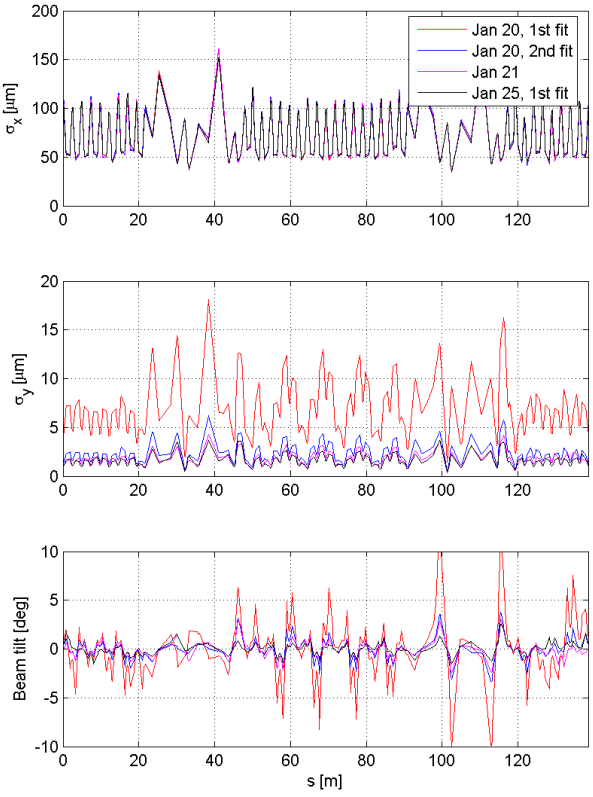

FIG. 26: Equilibrium horizontal and vertical beam sizes and beam tilt calculated from the lattice models fitted to successive sets of ORM data.

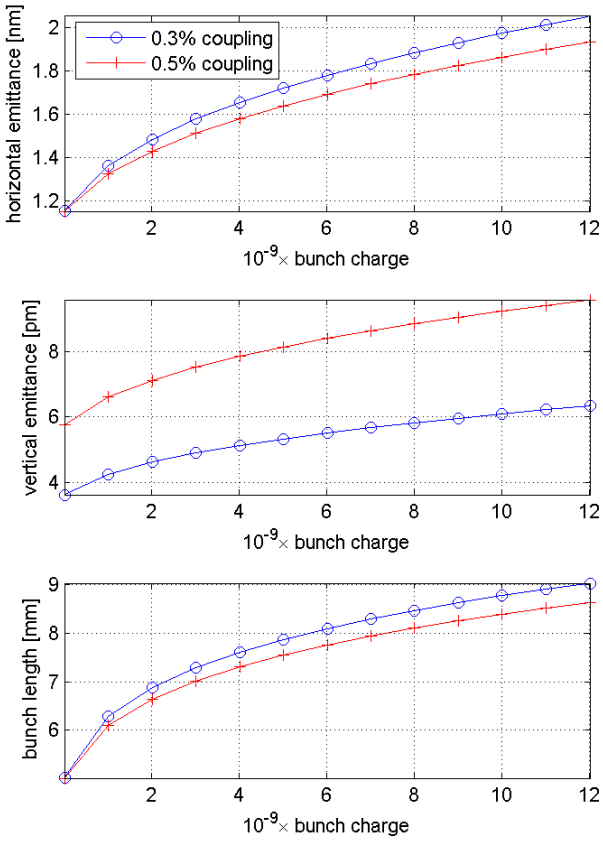

FIG. 27: Growth in horizontal emittance, vertical emittance and bunch length with increasing bunch charge, resulting from intrabeam scattering.

with a zero-charge vertical emittance around 4 pm, but obtaining accurate results in this regime is difficult. To confirm the results, a more rigorous set of measurements over a range of beam currents would be necessary.

V. CONCLUSIONS

ORM analysis has been shown to be an effective tool in tuning the KEK-ATF for low vertical emittance. With the machine operating in a stable condition (i.e. with small variation in the pulse-to-pulse injected bunch charge), the necessary data can be collected and analyzed, and a coupling correction calculated and applied, in less than three hours. The ORM analysis also provides potentially useful information on the BPM gains and couplings, as well as on focusing errors in the lattice. The coupling correction we were able to achieve may have been limited by the available current for the skew quadrupole trim windings used to apply the correction. Nevertheless, measurements of dispersion, beam lifetime and vertical beam size were consistent with a reduction in the vertical emittance by a factor of two compared to the starting point, with a bunch charge of 7×10^9. The vertical beam size measurement indicates a vertical emittance of around 6 pm at this charge after coupling correction based on ORM analysis. If IBS is taken into account, the zero-charge vertical emittance may have been around 4 pm.

Further improvements in the coupling correction will be necessary before it is possible to achieve the vertical emittance of 2 pm specified for the ILC. It is hoped that stabilization of the beam energy and compensation of the current dependence of the BPMs will go some way towards this. Steering to center the beam in the sextupoles (using beam-based alignment techniques) may help to reduce the skew quadrupole trim currents needed for coupling correction, and in particular keep the necessary skew quadrupole strengths within the range of the power supplies. We hope to address these issues in future studies.

Acknowledgements

We thank our hosts at KEK during our visit, for invaluable support and assistance with this work. We also thank J. Safranek (SSRL), A. Terebilo (SSRL), G. Portmann (LBNL) and C. Steier (LBNL) for developing the tools we used, and for useful discussions and advice.

[1] http://www-atf.kek.jp/atf/
[2] Y. Honda *et al.*, "Achievement of Ultralow Emittance Beam in the Accelerator Test Facility Damping Ring," Phys. Rev. Lett. **92**, 054802 (2004).
[3] C. Steier *et al.*, "Coupling Correction and Beam Dynamics at Ultralow Vertical Emittance in the ALS," Proceedings of the 2003 Particle Accelerator Conference, Portland, Oregon (2003).
[4] A. Wolski *et al.*, "Analysis of KEK-ATF Optics and Coupling Using LOCO," Proceedings of EPAC 2004, Lucerne, Switzerland (2004).
[5] A. Wolski *et al.*, "Analysis of KEK-ATF Optics and Coupling Using LOCO," ATF Report, ATF-03-09 (2004).
[6] J. Safranek *et al.*, "Matlab-Based LOCO," Proceedings of EPAC 2002, Paris, France (2002).
[7] H. Wiedemann, "Particle Accelerator Physics II," p. 329, Springer (1995).
[8] M. S. Zisman, in "Handbook of Accelerator Physics and Engineering," (Eds. A.W. Chao and M. Tigner) p. 218, World Scientific (1999).
[9] A. Terebilo, "Accelerator Toolbox for Matlab," SLAC-PUB-8732 (2001). http://www-ssrl.slac.stanford.edu/at/